

Universality of Heisenberg-Ising chain in external fields

Haiyuan Zou,¹ Rong Yu,^{2,*} and Jianda Wu^{1,†}

¹*Tsung-Dao Lee Institute & School of Physics and Astronomy,
Shanghai Jiao Tong University, Shanghai 200240, China*

²*Department of Physics and Beijing Key Laboratory of Opto-electronic Functional Materials & Micro-nano Devices,
Renmin University of China, Beijing, 100872, China*

Motivated by the recent surge of transverse-field experiments on quasi-one-dimensional antiferromagnets Sr(Ba)Co₂V₂O₈, we investigate the quantum phase transition in a Heisenberg-Ising chain under a combination of two in-plane inter-perpendicular transverse fields and a four-period longitudinal field, where the in-plane transverse field is either uniform or staggered. We show that the model can be unitary mapped to the one-dimensional transverse-field Ising model (1DTFIM) when the x and y components of the spin interaction and the four-period field are absent. When these two terms are present, following both analytical and numerical efforts, we demonstrate that the system undergoes a second-order quantum phase transition with increasing transverse fields, where the critical exponents as well as the central charge fall into the universality of 1DTFIM. Our results naturally identify the 1DTFIM universality of 1D quantum phase transitions observed in the existed experiments in Sr(Ba)Co₂V₂O₈ with transverse field applied along either [100] or [110] direction. Upon varying the tuning parameters a critical surface with 1DTFIM universality is determined and silhouetted to exhibit the general presence of the universality in a much wider scope of models than conventional understanding. Thus our results provide a broad guiding framework to facilitate the experimental realization of 1DTFIM universality in real materials.

I. INTRODUCTION

Quantum phase transition arises when the ground state energy of a many-body system encounters non-analyticity upon non-thermal parameter tuning^{1,2}. A quantum critical point (QCP) pops up when the transition is continuous. Near a QCP, exotic behaviors which have no counterparts in classical phase transitions emerge due to the intrinsic driven power of quantum fluctuations. These include the non-Fermi-liquid behavior and unconventional superconductivity in a variety of strongly correlated electron systems^{1,3-8}, as well as the peculiar spin dynamics in one-dimensional quantum magnets^{9,10}.

The one-dimensional transverse-field Ising model (1DTFIM) serves as a paradigmatic quantum spin model that exhibits a continuous quantum phase transition with rich quantum critical behaviors¹¹⁻¹⁹, where the celebrated conformal invariance emerges near its QCP²⁰. Although the quantum criticality of the 1DTFIM has been theoretically studied in great detail during past decades, it remains rare and tough to experimentally detect this 1D quantum criticality: On one hand, spin interactions beyond the standard 1DTFIM are usually non-negligible in real materials; on the other hand, the 3D ordering at finite temperatures may mask the 1D quantum critical point and the associated critical behavior²¹.

Among the potential materials, the widely investigated quasi-one-dimensional effective spin-1/2 antiferromagnetic Heisenberg-Ising screw chain compounds SrCo₂V₂O₈ (SCVO)²²⁻²⁶ and BaCo₂V₂O₈ (BCVO)²⁷⁻³¹ are encouraging candidates to access the 1D QCP. Recent series transverse-field experiments on these two materials confirm the existence of a novel 1D QCP residing outside the dome of the 3D Néel ordered phase, which further reveals promising features of quantum criticality of

1DTFIM universality around the 1D QCP^{19,32}. However, the underlying effective model for understanding this 1D QPT is complicated. Owing to the screw chain structure, the applied transverse field induces an in-plane staggered field perpendicular to it and a four-period field along the crystalline c axis. This gives rise to a Heisenberg-Ising model under various external fields [*cf.* Eq. (1)].

This superficially complicated model looks completely different from the original 1DTFIM. It raises a question about the nature of the QCP, if there exists one, in the model [*cf.* Eq. (1)]. To clarify this issue, we systematically carry out theoretical investigation on the quantum phase transition and the possible universality class near the QCP of the effective model via determining various critical exponents as well as the central charge associated with the conformal invariance.

Application of a transverse magnetic field suppresses the long-range antiferromagnetic (AF) order and induces an order-disorder phase transition. As a consequence of the anisotropy of the crystal structure, the value of the critical transverse field varies with the field direction. For example, when the transverse field is applied along the [100] direction, a staggered transverse field along the [010] direction and a four-period-staggered field along the [001] direction (c axis) are induced³¹. The induced fields shift the quantum critical point H_c to ~ 10 T for BCVO³³ and ~ 7 T for SCVO³⁴, significantly lower than the H_c values when the field is applied along the [110] direction¹⁹. Given that the interchain exchange coupling is much weaker than the intrachain coupling along the easy-axis (c -axis) in these compounds, these order-disorder phase transitions exhibit sharp features and can be described by an effective 1D spin-1/2 XXZ model with external fields.

In this paper, we study this effective 1D model [*cf.*

Eq. (1)] with corresponding parameters following the existed materials of SCVO and BCVO. By using infinite time-evolving block decimation (iTEBD) method^{35,36}, we calculate the staggered magnetization, the entanglement entropy, and the spin-spin correlation function with fields to locate the QCP. Meanwhile, the scaling analysis on these quantities allows us to extract various critical exponents and the central charge to characterize the nature of the quantum phase transition. The phase transition is found to fall into the 1DTFIM universality for the transverse field applied along the [100] (or equivalently [010]) direction in real experiments³². We further demonstrate that the induced c -axis four-period-staggered field is irrelevant for the universality of the transition. After pinning down the nature of the 1D QCP in the existed transverse-field experiments on SCVO and BCVO, more general situations of the model are further analyzed in detail by relaxing the allowed tuning fields in the effective model. With varying the spin anisotropy factor ϵ and the transverse components of the g factor g_x and g_y , a critical surface falling into 1DTFIM universality is determined and silhouetted in the parameter space. The numerical calculation is subsequently followed by a mean field analysis, which qualitatively confirms the iTEBD results for small ϵ . The well-established critical surface immediately leads to promising prediction that a line of 1DTFIM critical point should be directly observed when the transverse field is gradually rotated from [100] to [110] direction in either SCVO or BCVO.

The rest of this paper is organized as follows. Sec. II presents the effective model for SCVO and BCVO, and shows that the quantum phase transition induced by tuning the applied transverse field belongs to the 1DTFIM universality class. Sec. III studies the model in more general situations. We obtain the ground-state phase diagram of this generalized model by iTEBD calculations. These numerical results are further confirmed by a mean-field analysis. Sec. IV provides a guideline for experiments based on the general theoretical results. We draw conclusion in Sec. V.

II. THE EFFECTIVE MODEL

For the material of SCVO or BCVO when the transverse field is applied along the [100] direction, the corresponding effective spin-1/2 Heisenberg-Ising XXZ Hamiltonian reads as

$$H = \sum_i J[\epsilon(S_i^x S_{i+1}^x + S_i^y S_{i+1}^y) + S_i^z S_{i+1}^z] - g \sum_i [S_i^x + h_y(-1)^i S_i^y + h_z \cos(\pi \frac{2i-1}{4}) S_i^z], \quad (1)$$

where $\vec{S} = \vec{\sigma}/2$, and $\vec{\sigma}$ refer to the three Pauli matrices. Take the SCVO system for example, $J = 1.67$ meV, and the anisotropic factor $\epsilon \sim 0.5$ are estimated³⁷. $g = \mu_B G_x h$ with Bohr magneton μ_B , the gyromagnetic

ratio $G_x = 2.79$,³⁷ and h is the applied a -axis magnetic field. The ratio of the induced staggered fields to g are set as $h_{y(z)} = 0.4(0.14)$ ³¹. In our calculation, we set the energy unit $J = 1$ in the model, and take the anisotropic factor $\epsilon = 0.47$. In this way, g is the only tuning parameter in the model.

At small magnetic fields the ground state of the model is an antiferromagnetic (AF) ordered state. The applied magnetic field in [100] direction plays the role of suppressing this order, and gives rise to a quantum phase transition at a QCP, g_c . The induced staggered h_y field enhances this effect, while the h_z field has negligible contribution. To see this, we calculate the average magnetization in z direction, M_z , using the iTEBD method for the Hamiltonian in Eq. (1) for two cases: with and without the h_z term. We find that the h_z term indeed only slightly changes the location of the QCP: As shown in Fig. 1(a), the critical field $g_{c1} = 0.1454(1)$ in the former case, and $g_{c2} = 0.1456(1)$ for the latter. The critical exponent β can be obtained by fitting $M_z \sim |g_{ci} - g|^\beta$ ($i = 1, 2$) for both cases. In Fig. 1(a) the fitting gives $\beta = 0.126(5)$ and $0.128(5)$ for the two cases, both agree with $\beta \sim 1/8$ of the 1DTFIM universality within error bars. We also calculate the entanglement entropy $S(l) = -\text{Tr} \rho_A \ln \rho_A$ for a subsystem A with l spins in an infinite chain, where the reduced density matrix of A is defined as $\rho_A = \text{Tr}_B |\Psi_A \otimes \Psi_B\rangle \langle \Psi_A \otimes \Psi_B|$. (The ground state wavefunction can be decoupled to the tensor product of wavefunctions of subsystems, Ψ_A and Ψ_B). From conformal field theory analysis³⁸, the entanglement entropy scales as $S(l) = \frac{c}{3} \ln l + \text{const}$, where c is the central charge associated with the conformal invariance. Figure 1(b) shows the scaling of $S(l)$ with subsystem size l , which gives $c = 0.502(5)$ and $c = 0.503(5)$, for both cases with and without the h_z term, respectively. Note that either agrees with $c = 1/2$ of the 1DTFIM. The critical exponent β and central charge c are consistent with Ref.³⁹ where only the staggered field (h_y term) is considered. We further calculate the spin-spin correlation, denoted as $C(i-j) = \langle S_i^z S_j^z \rangle - \langle S_i^z \rangle \langle S_j^z \rangle$, for Hamiltonian Eq. (1) with and without the h_z term (see Fig. 1(c)). Using the relation $C(i-j) = e^{-|i-j|/\xi}$, with correlation length ξ and $1/\xi \sim |g_c - g|^\nu$, the critical exponent ν can be obtained. We find $\nu = 0.986$ (0.990) ~ 1 for the cases with (without) h_z term (Fig. 1d).

Based on these evidences, we conclude: (1) The quantum phase transition falls in the 1DTFIM universality class; (2) the four-period z field is an irrelevant term for this transition, which only slightly shifts the location of the QCP. For the case when the transverse field is applied along the [110] direction in some experimental setup, after some slight modifications, the model in Eq. (1) can still describe the phase transition. In this case, we need to set $h_y = 0$, and take the h_z term to be $\cos(\frac{\pi(i-1)}{2}) S_i^z$ for spin on site i , with a four-period $\uparrow 0 \downarrow 0$ pattern³¹. Compare with the four-period $\uparrow \downarrow \downarrow \uparrow$ pattern for the [100] cases, the effects of the $\uparrow 0 \downarrow 0$ pattern of the h_z term is even weaker. In particular, the quantum phase transition

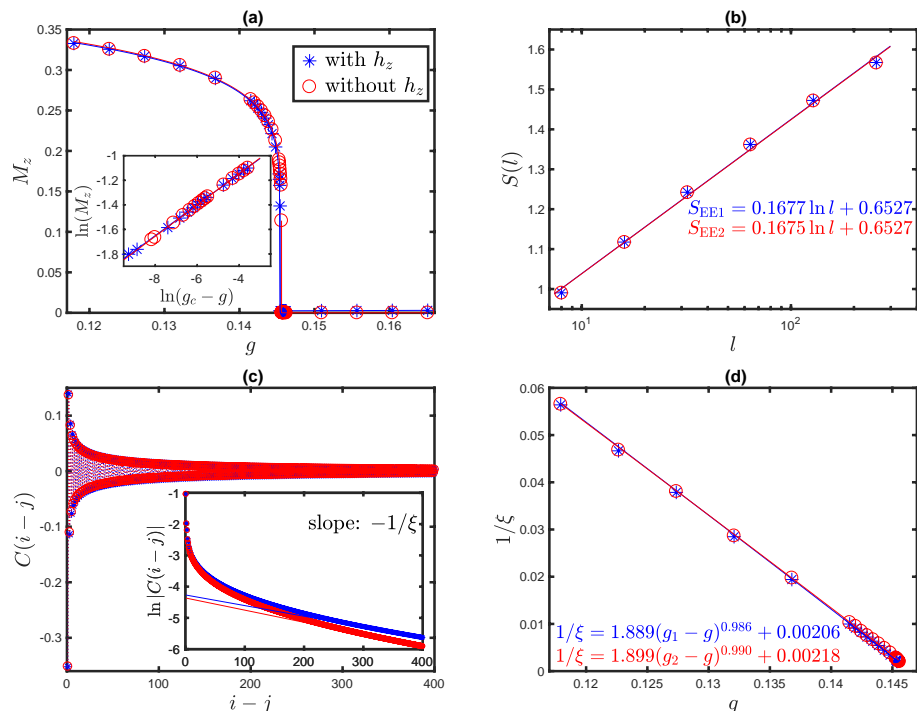


FIG. 1. Results from iTEBD calculation: (a) The average of staggered magnetization M_z vs. g for cases with (blue) and without (red) the h_z term. The curves are fits to $M_z = 0.524(g_{c1} - g)^{0.126}$ and $M_z = 0.530(g_{c2} - g)^{0.128}$ for the two cases, respectively, where the critical points $g_{c1} = 0.1454$ and $g_{c2} = 0.1456$. In either case $\beta \sim 1/8$ is obtained within error bar. The inset shows the scaling plot of M_z in the log-log scale. (b) Entanglement entropy $S_{EE}(l)$ vs. chain segment length l in the semi-log scale. In either case the slope value agrees with a central charge of $c \sim 1/2$. (c) Spin-spin correlation function $C(i-j)$ vs. distance $i-j$ at $g = 0.1448$ (near the QCP). The inset indicates that $\ln|C(i-j)|$ is proportional to $i-j$ at large distance. (d) The inverse of correlation length $1/\xi$ vs. g , where both cases give $\nu \sim 1$.

still keeps the 1DTFIM universality.

III. THE GENERALIZED MODEL

Since the small h_z term in Eq. (1) is irrelevant to the quantum phase transition induced by the transverse field, we drop the h_z term and focus on the effects of the two inter-perpendicular transverse fields via studying a generalized model from the Hamiltonian in Eq. (1).

$$H_g = \sum_i J[\epsilon(S_i^x S_{i+1}^x + S_i^y S_{i+1}^y) + S_i^z S_{i+1}^z] - \sum_i [g_x S_i^x + g_y (-1)^i S_i^y] \quad (2)$$

with $\epsilon < 1$. We consider arbitrary ratio g_y/g_x . It extends the parameter region of the realistic model Eq. (1) in Sec. II, where the ratio $h_y = g_y/g_x$ is fixed as 0.4. For small g_x and g_y , the Hamiltonian Eq. (2) has an AF ordered ground state.

A. iTEBD calculation

We first use the iTEBD method to study the model Eq. (2) extensively. The average magnetization M_z for various g_x and g_y values is calculated, and the quantum critical point is reached when the AF ordering is completely suppressed.

We scan the parameters g_x and g_y with $\epsilon = 0, 0.1, \dots, 1$, and obtain the QCPs of the generalized model in a 3D g_x - g_y - ϵ parameter space. As shown in Fig. 2, the obtained QCPs form a smooth critical surface. At $\epsilon = 0$, *i.e.* without the XY spin interaction terms, the critical points in the g_x - g_y plane are located on a circle with $|g_c| = 0.5$ since in this case the model can be unitary transformed to the 1DTFIM. At a small ϵ , the critical points approximately form an ellipse with $g_{cx} > g_{cy}$, where $g_{c(x,y)}$ is the critical point on the $x(y)$ axis. For $\epsilon \geq 0.4$, a nonmonotonic behavior of the critical curve appears due to the nontrivial competition among the XY spin interactions, g_x , and g_y terms. The critical curve forms a dumbbell shape with $g_{cx} \gg g_{cy}$. g_{cy} continuously shrinks with increasing ϵ and vanishes at $\epsilon = 1$ and $g_{cx} = 2$. When $\epsilon = 1$, the XXZ Heisenberg-Ising Hamiltonian becomes the Heisenberg XXX model. Without the external fields, the XXX model naturally contains an $SU(2)$ symmetry

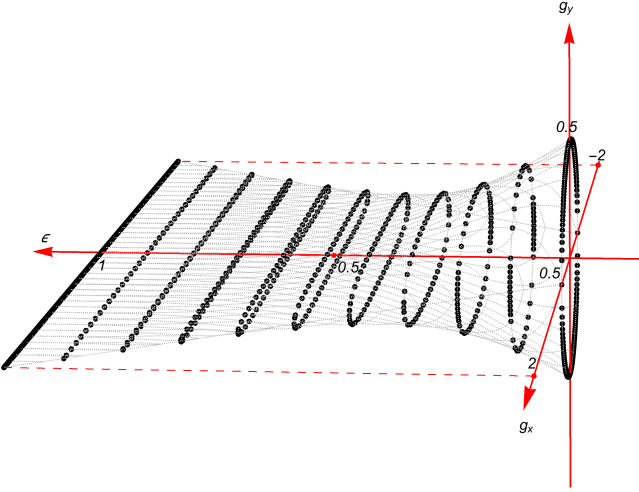


FIG. 2. The critical surface of the generalized model in Eq. (2) in the 3D parameter space from iTEBD calculation.

with no long-range magnetic order at zero temperature. Therefore, at $\epsilon = 1$ the external fields just simply lead to paramagnetic response. We notice that the 1DTFIM-type QCP obtained from Sec. II falls into this critical surface. By checking the linearity between the magnetization M_z^8 and $g_{x,y}$ across the QCPs on the critical surface, we can conclude that the transition across any point on the critical surface belongs to the 1DTFIM universality class. The critical surface is symmetric along the x (or y) axis as the Hamiltonian is invariant by sending $S^{x(y)} \rightarrow -S^{x(y)}$ when $g_{x(y)} \rightarrow -g_{x(y)}$. For $\epsilon > 1$, the XXZ model will become Heisenberg-XY type with physics dominated by the XY term. The influence of various external fields at this situation will be deferred to future study.

B. Mean field calculation

To further understand the properties of the phase transition obtained from iTEBD calculation, a π rotation of spins on even sites ($U = \exp[-i\pi \sum_j S_{2j}^z]$) are carried out to transform the Hamiltonian [Eq. (2)] into

$$H'_g = \sum_i J[\epsilon(S_i^x S_{i+1}^x - S_i^y S_{i+1}^y) - S_i^z S_{i+1}^z] - \sum_i [g_x S_i^x + g_y S_i^y]. \quad (3)$$

Correspondingly, the AF ground state at small g_x and g_y values for Eq. (2) is transferred to a Ferromagnetic (FM) state. Due to the asymmetric ϵ terms in Eq. (3), the perturbation of g_x and g_y is nonequivalent. Both the ϵ and $g_{x,y}$ terms suppress the FM state, but the $g_x S_i^x$ term competes with $\epsilon S_i^x S_{i+1}^x$. It can induce a reentrant

behavior of the staggered magnetization in the transverse XXZ model with $g_y = 0$, which is discussed in Ref⁴⁰ for $\epsilon \geq 0.4$. However, the $g_y S_i^y$ and $-\epsilon S_i^y S_{i+1}^y$ terms have similar effects. Thus, adding a g_y term can efficiently suppress the FM phase. This also means the staggered y -field can greatly assist to destroy the AF ordering in the original model [Eq. (2)].

We then carry out a mean field treatment^{41,42} to the generalized model [Eq. (3)]. Here, another unitary transformation, rotating the spins around the z axis by θ , is performed, before rotating all the spins around the x axis by $\pi/2$. Through these two transformation, magnetic field is directed along a new z axis contributed from both g_x and g_y terms. After a Jordan-Wigner transformation, a spinless fermion Hamiltonian is obtained,

$$H'' = \sum_i \frac{J_+}{2} (a_i^\dagger a_{i+1} + \text{h.c.}) + \frac{J_-}{2} (a_i^\dagger a_{i+1}^\dagger + \text{h.c.}) - \gamma(n_i - 1/2)(n_{i+1} - 1/2) + g_0(n_i - 1/2) \quad (4)$$

with $J_\pm = (\gamma \pm 1)/2$, $\gamma = \epsilon \cos(2\theta)$, $g_0 = g_x \sin \theta + g_y \cos \theta$, and $n_i = a_i^\dagger a_i$ is the density operator. The four-fermion interaction term is decoupled in three possible ways, with the expectation values for the magnetization, kinetic hopping, and pairing terms denoted as

$$M = \langle n_i \rangle - 1/2, K = \langle a_{i+1}^\dagger a_i \rangle, P = \langle a_{i+1} a_i \rangle. \quad (5)$$

The mean-field Hamiltonian then becomes

$$H_{\text{MF}} = \sum_i [\frac{\tilde{J}_+}{2} a_i^\dagger a_{i+1} + \frac{\tilde{J}_-}{2} a_i^\dagger a_{i+1}^\dagger + \text{h.c.} + \tilde{g}(n_i - 1/2)], \quad (6)$$

where

$$\tilde{J}_+ = J_+ + 2\gamma K, \tilde{J}_- = J_- - 2\gamma P, \tilde{g} = g_0 - 2\gamma M. \quad (7)$$

Fourier transform the Hamiltonian to the momentum space and diagonalize it using a Bogoliubov transformation,

$$a_k = u_k \alpha_k + v_k \alpha_{-k}^\dagger, a_{-k}^\dagger = -v_k^* \alpha_k + u_k \alpha_{-k}^\dagger \quad (8)$$

with

$$u_k = \sqrt{(1 + \frac{\tilde{J}_+ \cos k + \tilde{g}}{\omega(k)})/2}, v_k = i \text{sgn}(k) \sqrt{(1 - \frac{\tilde{J}_+ \cos k + \tilde{g}}{\omega(k)})/2}.$$

The mean field Hamiltonian density becomes

$$H_{\text{MF}}/N = \int_0^\pi \frac{dk}{2\pi} [\frac{1}{2} \tilde{J}_+ \cos k + \omega(k)(\alpha_k^\dagger \alpha_k - \frac{1}{2})] + \gamma M^2 - \gamma K^2 + \gamma P^2, \quad (9)$$

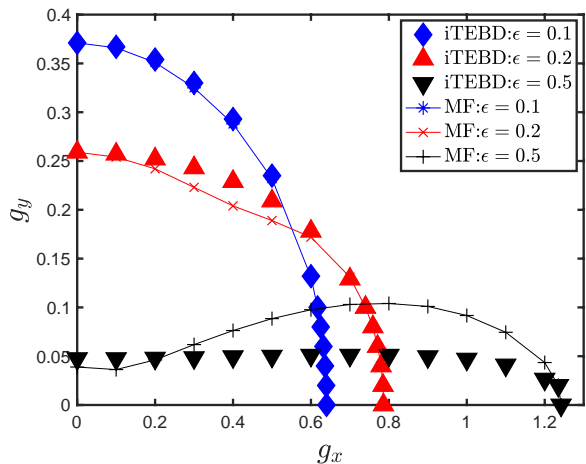


FIG. 3. Critical line in the g_x - g_y plane at $\epsilon = 0.1, 0.2$ and 0.5 from mean-field calculation (lines) and iTEBD (points).

where $\omega(k)$ is the single particle excitation spectrum,

$$\omega(k) = \sqrt{(\tilde{J}_+ \cos k + \tilde{g})^2 + (\tilde{J}_-)^2}. \quad (10)$$

The quantities M, K, P can be determined by the self-consistency conditions:

$$\begin{aligned} M &= - \int_0^\pi \frac{dk}{2\pi} \frac{\tilde{J}_+ \cos k + \tilde{g}}{\omega(k)}, \\ K &= - \int_0^\pi \frac{dk}{2\pi} \frac{(\tilde{J}_+ \cos k + \tilde{g}) \cos k}{\omega(k)}, \\ P &= - \int_0^\pi \frac{dk}{2\pi} \frac{\tilde{J}_- \sin^2 k}{\omega(k)}, \end{aligned}$$

and the optimized θ can be fixed by minimizing the ground state energy.

The phase diagram in g_x - g_y plane for a few different ϵ values is shown in Fig. 3. For small ϵ , the critical line is consistent with that determined from the iTEBD method. For $\epsilon = 0.5$, the nonmonotonic behavior of the transition line is also observed at mean-field level, although the critical line determined is quantitatively deviated from the iTEBD results.

We can understand the different critical line shapes at small and large ϵ values within the mean-field approach. For small $\epsilon \leq 0.2$, there is only one optimized θ value from 0 to $\pi/2$, while the parameter g_x and g_y are tuned from $(g_x = 0, g_y > 0)$ to $(g_x > 0, g_y = 0)$. The single particle spectrum function $\omega(k)$ is gapless at $k = 0$ at the order-disorder transition point (Fig. 4(a)). For intermediate $\epsilon \geq 0.5$, however, a double well structure of the energy as a function of θ appears (Fig. 4(b)), which indicates competing quantum fluctuations between the g_x and g_y terms. By fixing g_x , at $g_y < g_c$ where g_c is the critical point, the minimal energy point is closer to $\theta \sim \pi/2$, and thus $g_0 \sim g_x$. In this case, the g_x term dominates the critical quantum fluctuations. However, after g_y crosses

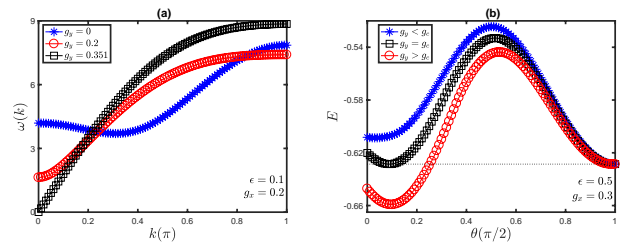


FIG. 4. (a) $\omega(k)$ as a function of k at $\epsilon = 0.1$ and $g_x = 0.1$ for $g_y = 0, 0.2$, and 0.351 (transition point). (b) Double well structure of the energy as a function of θ at $\epsilon = 0.5$ and $g_x = 0.3$ for varied $g_y < g_c$, $g_y = g_c$, and $g_y > g_c$, where g_c is the transition point

the critical point g_c , the minimal energy point jumps to $\theta \sim 0$ and thus $g_0 \sim g_y$, which indicates that the g_y term begins to play the major role. We fix the phase transition boundary at the point g_c where the ground-state degenerate appears. The above analysis based on the introduced optimized θ gives a qualitative explanation of the novel behavior of the critical curve in the g_x - g_y plane for large ϵ . At large ϵ , the quantum fluctuations due to the XY spin interaction term is highly relevant, while the interplay between the intrinsic fluctuations and the $g_{x,y}$ term makes the phase transition further nontrivial. In the mean-field treatment, the odd-order terms $a_i^\dagger a_i a_{i+1}$ via Jordan-Wigner transformation are neglected. The increasing discrepancy between the mean field analysis and the iTEBD results with increasing ϵ indicates these neglected non-linear terms play a non-negligible role, and eventually lead to the breakdown of the mean-field theory when $\epsilon \rightarrow 1$.

IV. GUIDANCE TO EXPERIMENTS

Because of the induced four-period z field is irrelevant, our extensive study of the phase transition on the generalized model with broad parameter region g_x and g_y provides a concrete guidance to the experiments on real materials of quasi-1D Ising anisotropic quantum magnets, such as SCVO and BCVO. In SCVO and BCVO, different g_y/g_x ratio can be realized by applying a transverse field which gradually rotates in the $x - y$ plane. The rotation of the applied transverse field shifts the position of the QCP. At the [100] direction, strongest in-plane staggered field g_y perpendicular to the external transverse one is induced. Deviation of the applied transverse field from the [100] direction weakens g_y . Consequently it requires stronger applied transverse field to reach the 1DTFIM QCP. And when the applied field reaches the direction of [110], the required external transverse field reaches maximum. This is clearly observed in BCVO¹⁹ and the recent NMR experiments on SCVO³² with the external transverse field applied along [110] and [100], respectively. For SCVO, when the field is applied to the [100] direction the 1D QCP of SCVO is slightly outside

the 3D ordered phase³². As the QCP(1D) will be pushed further by rotating the in-plane applied field, it can be used to distinguish unambiguously the 3D QCP and 1D QCP at [100] direction and provide a clean platform to examine the novel quantum critical behavior near the 1D QCP.

V. CONCLUSION

To conclude, following the corresponding effective one-dimensional Heisenberg-Ising model with axial anisotropy tuned by ϵ , we demonstrate that the observed transverse-field (h_x)-tuned quantum phase transition outside the three-dimensional Néel order in the materials of BCVO and SCVO falls into the 1DTFIM universality, despite of the presence of the induced in-plane staggered field (h_y) and the four-period fields along the c axis (h_z). Small h_z is further shown to make negligible effects on the phase transition. A generalized model is immediately constructed by neglecting h_z and relaxing the ϵ , h_x , and h_y to a broad parameter region. With the generalized model, the nature of quantum phase transitions is then extensively and carefully scrutinized by the iTEBD method, and it has been shown that the quantum phase transition falls into the 1DTFIM universality, rendering out a nice 1DTFIM quantum critical surface until $\epsilon = 1$ (XXX limit). The well-established 1DTFIM critical surface obtained from the generalized model is expected to guide the in-plane-field-rotation measurements on real materials such as SCVO, BCVO, and CoNb_2O_6 *etc.*. Our study concretely demonstrates that the 1DTFIM universality is robust against additional spin interaction terms as well as various external fields. This opens rich opportunities to access to the 1DTFIM QCP and realize the celebrated Zamolodchikov quantum E_8 integrable model⁴³ near this QCP in real materials.

VI. ACKNOWLEDGMENTS

We thank Weiqiang Yu and Zhe Wang for helpful discussions. The work at Shanghai Jiao Tong University is supported by the National Natural Science Foundation of China Grant No. 11804221 (H.Z.), and Science and Technology Commission of Shanghai Municipality Grant No. 16DZ2260200 (H.Z.). The work at Renmin University of China was supported by the Ministry of Science and Technology of China, National Program on Key Research Project Grant number 2016YFA0300504, the National Science Foundation of China Grant number 11674392, and the Fundamental Research Funds for the Central Universities and the Research Funds of Renmin University of China Grant number 18XNLG24 (R.Y.). J.W. acknowledges support from Shanghai city.

Appendix: iTEBD results

In this appendix, we list the values of the quantum critical points, used to generate the critical surface in Fig. 2 of the main text. In tables I-III, $[g_x, g_y]$ are the critical points in the g_x - g_y plane for different ϵ . All the critical points are obtained by scanning the parameter space along g_x or g_y with one of them held at fixed value. The width of error bars is the step size of the iTEBD calculation.

$\epsilon = 0.1$	$\epsilon = 0.2$	$\epsilon = 0.3$
[0, 0.371(1)]	[0, 0.259(1)]	[0, 0.166(1)]
[0.1, 0.367(1)]	[0.1, 0.257(1)]	[0.1, 0.166(1)]
[0.2, 0.354(1)]	[0.2, 0.252(1)]	[0.2, 0.164(1)]
[0.3, 0.330(1)]	[0.3, 0.243(1)]	[0.3, 0.161(1)]
[0.4, 0.293(1)]	[0.4, 0.229(1)]	[0.4, 0.157(1)]
[0.5, 0.235(1)]	[0.5, 0.209(1)]	[0.5, 0.151(1)]
[0.6, 0.132(1)]	[0.6, 0.178(1)]	[0.6, 0.141(1)]
[0.617(1), 0.1]	[0.7, 0.129(1)]	[0.7, 0.127(1)]
[0.625(1), 0.08]	[0.736(1), 0.1]	[0.8, 0.104(1)]
[0.631(1), 0.06]	[0.755(1), 0.08]	[0.9, 0.058(1)]
[0.636(1), 0.04]	[0.769(1), 0.06]	[0.932(1), 0.02]
[0.639(1), 0.02]	[0.778(1), 0.04]	[0.936(1), 0]
[0.639(1), 0]	[0.784(1), 0.02]	---
---	[0.786(1), 0]	---

TABLE I. Phase transition points in g_x - g_y plane from iTEBD calculation.

$\epsilon = 0.4$	$\epsilon = 0.5$	$\epsilon = 0.6$
[0, 0.095(1)]	[0, 0.0475(5)]	[0, 0.0190(5)]
[0.1, 0.095(1)]	[0.1, 0.0475(5)]	[0.1, 0.0190(5)]
[0.2, 0.095(1)]	[0.2, 0.0480(5)]	[0.2, 0.0195(5)]
[0.3, 0.095(1)]	[0.3, 0.0485(5)]	[0.3, 0.0200(5)]
[0.4, 0.095(1)]	[0.4, 0.0495(5)]	[0.4, 0.0210(5)]
[0.5, 0.094(1)]	[0.5, 0.0500(5)]	[0.5, 0.0220(5)]
[0.6, 0.092(1)]	[0.6, 0.0510(5)]	[0.6, 0.0230(5)]
[0.7, 0.089(1)]	[0.7, 0.0510(5)]	[0.7, 0.0240(5)]
[0.8, 0.083(1)]	[0.8, 0.0510(5)]	[0.8, 0.0250(5)]
[0.9, 0.074(1)]	[0.9, 0.0495(5)]	[0.9, 0.0255(5)]
[1.0, 0.057(1)]	[1.0, 0.0470(5)]	[1.0, 0.0260(5)]
[1.050(1), 0.04]	[1.1, 0.0410(5)]	[1.1, 0.0260(5)]
[1.080(1), 0.02]	[1.2, 0.0265(5)]	[1.2, 0.0245(5)]
[1.089(1), 0]	[1.220(1), 0.02]	[1.3, 0.0205(5)]
---	[1.242(1), 0]	[1.380(1), 0.01]
---	---	[1.394(1), 0]

TABLE II. Phase transition points in g_x - g_y plane from iTEBD calculation (continue).

Technically, convergent iTEBD results upto particular

$\epsilon = 0.7$	$\epsilon = 0.8$	$\epsilon = 0.9$
[0, 0.0056(2)]	[0, 0.0016(2)]	[0, 0.0004(2)]
[0.1, 0.0058(2)]	[0.1, 0.0016(2)]	[0.1, 0.0004(2)]
[0.2, 0.0060(2)]	[0.2, 0.0018(2)]	[0.2, 0.0004(2)]
[0.3, 0.0064(2)]	[0.3, 0.0020(2)]	[0.3, 0.0004(2)]
[0.4, 0.0070(2)]	[0.4, 0.0020(2)]	[0.4, 0.0004(2)]
[0.5, 0.0074(2)]	[0.5, 0.0022(2)]	[0.5, 0.0004(2)]
[0.6, 0.0080(2)]	[0.6, 0.0022(2)]	[0.6, 0.0004(2)]
[0.7, 0.0086(2)]	[0.7, 0.0024(2)]	[0.7, 0.0004(2)]
[0.8, 0.0094(2)]	[0.8, 0.0026(2)]	[0.8, 0.0006(2)]
[0.9, 0.0100(2)]	[0.9, 0.0030(2)]	[0.9, 0.0006(2)]
[1.0, 0.0108(2)]	[1.0, 0.0032(2)]	[1.0, 0.0006(2)]
[1.1, 0.0114(2)]	[1.1, 0.0036(2)]	[1.1, 0.0006(2)]
[1.2, 0.0120(2)]	[1.2, 0.0038(2)]	[1.2, 0.0008(2)]
[1.3, 0.0120(2)]	[1.3, 0.0042(2)]	[1.3, 0.0008(2)]
[1.4, 0.0116(2)]	[1.4, 0.0044(2)]	[1.4, 0.0008(2)]
[1.5, 0.0086(2)]	[1.5, 0.0046(2)]	[1.5, 0.0010(2)]
[1.536(1), 0.005]	[1.6, 0.0042(2)]	[1.6, 0.0010(2)]
[1.547(1), 0]	[1.690(1), 0.002]	[1.7, 0.0010(2)]
---	[1.698(1), 0]	[1.8, 0.0008(2)]
----	----	[1.849(1), 0]

TABLE III. Phase transition points in g_x - g_y plane from iTEBD calculation.

significant digit can be reached as the Schmidt rank χ which characterizes the entanglement of the system is increased. In Sec. II, we carry the iTEBD calculation with $\chi = 10, 20, \dots, 70$ to obtain convergent four significant digit results for QCP locations. However, To obtain convergent three significant digit results, $\chi = 20$ is enough. Thus, the numerous QCP results in Sec. III is calculated from $\chi = 20$.

- * rong.yu@ruc.edu.cn
† wujd@sjtu.edu.cn
- ¹ Special issue on Quantum Phase Transitions, *J. Low Temp. Phys.* **161**, 1 (2010).
 - ² S. Sachdev, *Quantum phase transitions*, second ed. ed. (Cambridge University Press, Cambridge, 2011).
 - ³ Q. Si, S. Rabello, K. Ingersent, and J. L. Smith, *Nature* **413**, 804 (2001).
 - ⁴ A. Schröder, G. Aeppli, R. Coldea, M. Adams, O. Stockert, H. Löhneysen, E. Bucher, R. Ramazashvili, and P. Coleman, *Nature* **407**, 351 (2000).
 - ⁵ P. Coleman and A. J. Schofield, *Nature* **433**, 226 (2005).
 - ⁶ Q. Si and F. Steglich, *Science* **329**, 1161 (2010).
 - ⁷ E. Schubert, M. Tippmann, L. Steinke, S. Lausberg, A. Steppke, M. Brando, C. Krellner, C. Geibel, R. Yu, Q. Si, *et al.*, *Science* **351**, 485 (2016).
 - ⁸ J. Wu, Q. Si, and E. Abrahams, *Physical Review B* **93**, 104515 (2016).
 - ⁹ A. W. Kinross, M. Fu, T. J. Munsie, H. A. Dabkowska, G. M. Luke, S. Sachdev, and T. Imai, *Phys. Rev. X* **4**, 031008 (2014).
 - ¹⁰ J. Wu, M. Kormos, and Q. Si, *Phys. Rev. Lett.* **113**, 247201 (2014).
 - ¹¹ T. Niemeijer, *Physica* **36**, 377 (1967).
 - ¹² P. Pfeuty, *Annals of Physics* **57**, 79 (1970).
 - ¹³ E. Barouch and B. M. McCoy, *Phys. Rev. A* **3**, 786 (1971).
 - ¹⁴ M. Suzuki, *Prog. Theor. Phys.* **46**, 1337 (1971).
 - ¹⁵ M. Suzuki, *Prog. of Theor. Phys.* **56**, 1454 (1976).
 - ¹⁶ R. Jullien, P. Pfeuty, J. N. Fields, and S. Doniach, *Phys. Rev. B* **18**, 3568 (1978).
 - ¹⁷ A. Kopp and S. Chakravarty, *Nat. Phys.* **1**, 53 (2005).
 - ¹⁸ J. Wu, L. Zhu, and Q. Si, *Phys. Rev. B* **97**, 245127 (2018).
 - ¹⁹ Z. Wang, T. Lorenz, D. I. Gorbunov, P. T. Cong, Y. Kohama, S. Niesen, O. Breunig, J. Engelmayer, A. Herman, J. Wu, K. Kindo, J. Wosnitza, S. Zherlitsyn, and A. Loidl, *Phys. Rev. Lett.* **120**, 207205 (2018).
 - ²⁰ A. Belavin, A. Polyakov, and A. Zamolodchikov, *Nucl. Phys. B* **241**, 333 (1984).
 - ²¹ R. Coldea, D. A. Tennant, E. M. Wheeler, E. Wawrzynska, D. Prabhakaran, M. Telling, K. Habicht, P. Smeibidl, and K. Kiefer, *Science* **327**, 177 (2010).
 - ²² Z. He, T. Taniyama, and M. Itoh, *Phys. Rev. B* **73**, 212406 (2006).
 - ²³ A. K. Bera, B. Lake, F. H. L. Essler, L. Vanderstraeten, C. Hubig, U. Schollwöck, A. T. M. N. Islam, A. Schneidewind, and D. L. Quintero-Castro, *Phys. Rev. B* **96**, 054423 (2017).
 - ²⁴ A. K. Bera, B. Lake, W.-D. Stein, and S. Zander, *Phys. Rev. B* **89**, 094402 (2014).
 - ²⁵ Z. Wang, J. Wu, W. Yang, A. K. Bera, D. Kamenskyi, A. T. M. N. Islam, S. Xu, J. M. Law, B. Lake, C. Wu, and A. Loidl, *Nature* **554**, 219 (2018).
 - ²⁶ Q. Faure, S. Takayoshi, S. Petit, V. Simonet, S. Raymond, L.-P. Regnault, M. Boehm, J. S. White, M. Månsson, C. Rüegg, P. Lejay, B. Canals, T. Lorenz, S. C. Furuya, T. Giamarchi, and B. Grenier, *Nature Physics* **14**, 716 (2018).
 - ²⁷ Z. He, T. Taniyama, T. Kyômen, and M. Itoh, *Phys. Rev. B* **72**, 172403 (2005).
 - ²⁸ S. Kimura, H. Yashiro, K. Okunishi, M. Hagiwara, Z. He,

- K. Kindo, T. Taniyama, and M. Itoh, *Phys. Rev. Lett.* **99**, 087602 (2007).
- ²⁹ B. Lake, D. A. Tennant, J.-S. Caux, T. Barthel, U. Schollwöck, S. E. Nagler, and C. D. Frost, *Phys. Rev. Lett.* **111**, 137205 (2013).
- ³⁰ M. Klanjšek, M. Horvatić, S. Krämer, S. Mukhopadhyay, H. Mayaffre, C. Berthier, E. Canévet, B. Grenier, P. Lejay, and E. Orignac, *Phys. Rev. B* **92**, 060408 (2015).
- ³¹ S. Kimura, K. Okunishi, M. Hagiwara, K. Kindo, Z. He, T. Taniyama, M. Itoh, K. Koyama, and K. Watanabe, *Journal of the Physical Society of Japan* **82**, 033706 (2013).
- ³² Y. Cui, H. Zou, N. Xi, Z. He, Y. X. Yang, L. Shu, G. Zhang, Z. Hu, T. Chen, R. Yu, J. Wu, and W. Yu, submitted, 2019.
- ³³ S. K. Niesen, G. Kolland, M. Seher, O. Breunig, M. Vallador, M. Braden, B. Grenier, and T. Lorenz, *Phys. Rev. B* **87**, 224413 (2013).
- ³⁴ Z. Wang, J. Wu, S. Xu, W. Yang, C. Wu, A. K. Bera, A. T. M. N. Islam, B. Lake, D. Kamenskyi, P. Gogoi, H. Engelkamp, N. Wang, J. Deisenhofer, and A. Loidl, *Phys. Rev. B* **94**, 125130 (2016).
- ³⁵ G. Vidal, *Phys. Rev. Lett.* **98**, 070201 (2007).
- ³⁶ R. Orús and G. Vidal, *Phys. Rev. B* **78**, 155117 (2008).
- ³⁷ Z. Wang, M. Schmidt, A. K. Bera, A. T. M. N. Islam, B. Lake, A. Loidl, and J. Deisenhofer, *Phys. Rev. B* **91**, 140404 (2015).
- ³⁸ P. Calabrese and J. Cardy, *Journal of Statistical Mechanics: Theory and Experiment* **2004**, P06002 (2004).
- ³⁹ S. Takayoshi, S. C. Furuya, and T. Giamarchi, *Phys. Rev. B* **98**, 184429 (2018).
- ⁴⁰ Y. Heida, K. Okunishi, and Y. Akutsu, *Phys. Rev. B* **64**, 224422 (2001).
- ⁴¹ D. V. Dmitriev, V. Y. Krivnov, A. A. Ovchinnikov, and A. Langari, *Journal of Experimental and Theoretical Physics* **95**, 538 (2002).
- ⁴² J.-S. Caux, F. H. L. Essler, and U. Löw, *Phys. Rev. B* **68**, 134431 (2003).
- ⁴³ A. Zamolodchikov, *Int. J. Mod. Phys. A* **4**, 4235 (1989).